Regenerative Therapy 25 (2024) 35–48

Contents lists available at ScienceDirect

Regenerative Therapy

journal homepage: http://www.elsevier.com/locate/reth

Original Article

Epigenetic mechanism of miR-26b-5p-enriched MSCs-EVs attenuates spinal cord injury

Jinghui Xu*, Zhenxiao Ren, Tianzuo Niu, Siyuan Li

Department of Spine Surgery, The First Affiliated Hospital, Sun Yat-sen University (Guangdong Provincial Key Laboratory of Orthopaedics and Traumatology), Guangzhou, 510080, China

ARTICLE INFO

Article history:
Received 14 August 2023
Received in revised form
11 October 2023
Accepted 26 October 2023

Keywords:
Spinal cord injury
Mesenchymal stem cell
Extracellular vesicles
miR-26b-5p
KDM6A

ABSTRACT

Mesenchymal stem cells (MSCs) and extracellular vesicles (EVs) are promising therapies for the treatment of spinal cord injury (SCI). This study sought to explore the epigenetic mechanism of miR-26b-5p-enriched MSCs-EVs in SCI. MSCs and MSCs-EVs were isolated and characterized. The SCI rat model was established, followed by Basso-Beattie-Bresnahan scoring and H&E staining. In vitro cell models were established in PC12 cells with lipopolysaccharide (LPS) treatment, followed by cell viability evaluation using CCK-8 assay. The levels of miR-26b-5p, lysine demethylase 6A (KDM6A), NADPH oxidase 4 (NOX4), reactive oxygen species (ROS), and inflammatory factors (TNF-α/IL-1β/IL-6) in tissues and cells were detected. The levels of cy3-lablled miR-26b-5p in tissues and cells were observed by confocal microscopy. The binding of miR-26b-5p to KDM6A 3′UTR and the enrichments of KDM6A and H3K27me3 at the NOX4 promoter were analyzed. MSCs-EVs attenuated motor dysfunction, inflammation, and oxidative stress in SCI rats. MSCs-EVs delivered miR-26b-5p into PC12 cells to reduce LPS-induced inflammation and ROS production and enhance cell viability. miR-26b-5p inhibited KDM6A, and KDM6A reduced H3K27me3 at the NOX4 promoter to promote NOX4. Overexpression of KDM6A or NOX4 reversed the alleviative role of MSCs-EVs in SCI or LPS-induced cell injury. Overall, MSCs-EVs delivered miR-26b-5p into cells to target the KDM6A/NOX4 axis and facilitate the recovery from SCI.

1. Introduction

Spinal cord injury (SCI) is a devastating neurological disorder causing motor, sensory and autonomic deficits, with its prevalence increasing from 236 to 1298 cases per million general populations for the past three decades [1]. The pathophysiology of SCI involves two phases: the initial, mechanical injury characterized by local hemorrhage, edema, and ischemia due to compression, distraction, or translocation of the spinal column, and the secondary injury resulting in fatal accumulation of reactive oxygen species (ROS) and glutamate, the release of inflammatory cytokines, and activation of proapoptotic signaling, which contributes to the expansion of the injury zone [2,3]. Despite advances in the understanding of SCI pathophysiology, the new neurogenerative therapies for SCI have not been developed for the past decades. Mesenchymal stem cells (MSCs) with origins of a variety of tissues (e.g., bone marrow, umbilical cord and placenta) have strong multi-directional differentiation ability [4]. MSCs are widely applied in clinical therapy due to their easy availability, genetic stability, poor immunogenicity, efficacy for tissue repair, hematopoiesis and immunomodulation

Abbreviations: SCI, Spinal cord injury; ROS, Reactive oxygen species; MSCs, Mesenchymal stem cells; EVs, Extracellular vesicles; miRNAs, MicroRNAs; KDM6A, Lysine demethylase 6A; H3K27, histone H3 lysine 27; 3′UTR, 3′ untranslated region; PBS, phosphate buffered saline; FBS, fetal bovine serum; TEM, transmission electron microscopy; NTA, nanoparticle tracking analyzer; BBB, Basso-Beattie-Bresnahan; LPS, Lipopolysaccharide; GFP, green fluorescent protein; TUNEL, Terminal deoxynucleotidyl transferase-mediated dUTP-biotin nick end labeling; DHE, Dihydroethidium; DCFDA, 2,7-dichlorofluorescein diacetate; ELISA, Enzyme-linked immunosorbent assay; TNF-α, tumor necrosis factor-α; IL, interleukin; qRT-PCR, Quantitative real-time polymerase chain reaction; ChIP, Chromatin immunoprecipitation; GAPDH, Glyceraldehyde-3-phosphate dehydrogenase; ANOVA, analysis of variance.

* Corresponding author. The First Affiliated Hospital, Sun Yat-sen University (Guangdong Provincial Key Laboratory of Orthopaedics and Traumatology), No.58 Zhongshan Second Road, Yuexiu District, Guangzhou City, 510080, Guangdong Province, China.

E-mail addresses: xujh39@mail.sysu.edu.cn (J. Xu), renzhx8@mail2.sysu.edu.cn (Z. Ren), xujh39@mail.sysu.edu.cn (T. Niu), lisy239@mail2.sysu.edu.cn (S. Li).

Peer review under responsibility of the Japanese Society for Regenerative Medicine.

https://doi.org/10.1016/j.reth.2023.10.005

[5]. Extracellular vesicles (EVs), a set of cell-derived membranous structures loaded with proteins, lipids, and nucleic acids, emerge as a new source in the field of regenerative and anti-inflammatory medicine [6]. Given the limitation of MSCs therapy because of tumorigenicity, poor longevity after implantation, and immune rejection, MSCs derived EVs (MSCs-EVs) are considered a safer and advanced option for SCI management [7,8]. However, the regulatory mechanism of MSCs-EVs in SCI is poorly understood.

MicroRNAs (miRNAs) are a major type of cargos delivered by EVs to the recipient cells and EVs-encapsulated miRNAs are given great interest for clinical implication [9]. miRNAs are small non-coding RNA molecules with the ability to negatively modulate gene expression at the posttranscriptional level [10]. Exosomal miRNAs participate in the development of SCI by regulating microglial polarization, mitochondrial function, and neuroinflammation [11–13]. The miR-26 family members including by miR-26a, miR-26b, miR-1297, and miR-4465 have been validated as the regulators of tumorigenesis, cardiovascular disease, and obesity [14–16]. Especially, miR-26b has been previously demonstrated to inhibit oligodendrocyte precursor cell differentiation and facilitate locomotor recovery post SCI by regulating adrenomedullin [17]. However, it is unknown whether EVs involves the shuttle of miR-26b in SCI pathology.

Epigenetic modifications that regulate gene expression without alterations of the primary DNA sequence lie behind the pathology of neuropathic trauma and pain, and neuroinflammation [18]. Lysine demethylase 6A (KDM6A) in the catalog of the KDM6 demethylase family specific for histone H3 lysine 27 (H3K27), reverses the occupation of the methyl group on di- and trimethylated H3K27 (H3K27me2/3) at the gene promoters [19]. Emerging data have shown that the depletion of KDM6A promotes intrinsic neural regeneration, vascular regeneration, and neural repair, thus benefiting functional recovery post SCI [20–22]. The imbalance between ROS and antioxidants participates in the functional and pathological impairment after SCI [23]. NADPH oxidases are a vital source for ROS, and NOX4 is a member of the NADPH oxidase family and plays a driving role in apoptosis, ROS production, and inflammatory responses post SCI [24,25]. Importantly, our bioinformatic data suggested that KDM6A 3′ untranslated region (3′UTR) is a target of miR-26b-5p and the ChIP assay verified the enrichment of KDM6A and H3K27me3 at the NOX4 promoter, suggesting that the interactions between miR-26b-5p and KDM6A and between KDM6A and NOX4 play a role in SCI pathology.

Based on the above background, we speculated that MSCs-EVs mediate the delivery of miR-26b-5p to regulate the KDM6A/NOX4 axis, thus alleviating SCI. Therefore, the objective of our current study is to decipher the regulatory mechanism of MSCs-EVs to exert curative effects post SCI, providing the rationale for the application of MSCs-EVs in SCI treatment.

2. Materials and methods

2.1. Culture and characterization of human umbilical cord MSCs

Collected fresh umbilical cords were treated within 6 h. Fresh umbilical cords were rinsed twice with phosphate buffered saline (PBS) containing penicillin and streptomycin to clean away umbilical cord blood. Next, umbilical cords were sliced into 1–2 mm fragments, suspended in Dulbecco's modified Eagle's medium premixed with 10 % fetal bovine serum (FBS), 5 % human serum and 1 % penicillin and streptomycin (v/v), and preserved in a humidified incubator at 37 °C with 5 % CO_2. Nonadherent cells were washed away by PBS, and the medium was replaced every 3 days. The appearance of well-developed fibroblast-like cell colonies was observed after 10 days. The tissue culture was treated with trypsin, passaged (undiluted), and further amplified in a new culture dish. Each donor of umbilical cord signed the written informed consent.

HucMSCs of the third generation were separated with trypsin (Gibco by Life technologies, Grand Island, NY, USA) and resuspended in PBS (1×10^6 cells/mL). Subsequently, 200 μL of cell suspension was incorporated into an Eppendorf tube and cultured in humidified air at 37 °C with 5 % CO_2. The expression levels of CD73 (1:200, ab239246, Abcam), CD90 (1:500, ab11155, Abcam, Cambridge, MA, USA), CD31 (1:200, ab27333, Abcam), and CD34 (1:200, ab18227, Abcam) were analyzed by flow cytometry.

After trypsinization, HucMSCs of the third generation were prepared into single-cell suspension, followed by seeding into the 6-well plates (1×10^5 cells/mL). According to the provided protocol, OriCell™ human MSCs osteogenic differentiation medium (Cyagen Biosciences, Shanghai, China) and OriCell™ human MSCs adipogenic differentiation medium (Cyagen Biosciences) were added to the wells for 24 days of culture to analyze cell potentials for osteogenic and adipogenic differentiation. The reagents for osteogenic and adipogenic differentiation assays were oil red O (CHEM-200002-I)) and alizarin red (CHEM-200010-G) respectively.

2.2. Extraction and identification of EVs

EVs were removed from the serum through 8 h of ultracentrifugation at 100,000 × *g*. When reaching 80 % confluence, the supernatant in the medium was discarded. After two washes with PBS, the cell culture was conducted with 10 % FBS medium free of EVs at 37 °C with 5 % CO_2 for 48 h. The collected supernatant underwent multiple rounds of centrifugation (10 min at 300 × *g* and 4 °C, 15 min at 2000 × *g* and 4 °C, 15 min at 5000 × *g* and 4 °C, 30 min at 12,000 × *g* and 4 °C) for removal of precipitates. After washing with PBS, the suspension also underwent multiple rounds of centrifugation (70 min at 12,000 × *g* and 4 °C, 70 min at 100,000 × *g* and 4 °C, 70 min at 100,000 × *g* and 4 °C) for collection of precipitates. HucMSCs were incubated with 10 % EVs-free PBS medium containing GW4869 (Sigma–Aldrich, Merck KGaA, Darmstadt, Germany), and the resultant conditioned medium served as the control (GW). EVs were incorporated with Rnase I (Thermo Fisher Scientific Inc., Waltham, MA, USA) and Triton X-100 and thermally inactivated, followed by detection of miR-26b-5p in EVs.

Transmission electron microscopy (TEM) and NanoSight nanoparticle tracking analysis (NTA; Malvern Instruments, Worcestershire, UK) were applied to analyze the size and concentration of EVs. The surface makers of EVs were identified by means of Western blot. The total protein content in concentrated EVs suspension was quantified with application of a bicinchoninic acid assay kit (23,227, Thermo Fisher Scientific, Waltham, MA, USA). Protein samples were separated after 10 % sodium dodecyl sulfate polyacrylamide gel electrophoresis and then loaded to the membranes, followed by detection of specific EVs protein markers CD9 (1:1000, ab307085, Abcam), CD63 (1:1000, ab271286, Abcam), and the negative control Calnexin (1:1000, ab227310, Abcam).

2.3. Cell transfection

The assay kits used for lentivirus package, lentiviruses containing miR-26b-5p, and the negative control (NC) were procured from GeneCopeia (Rockville, Bethesda, MD, USA). Subsequently, HucMSCs were infected with lentiviral particles (5×10^8 TU/mL) for 24 h. After 48 h of culture, the stably infected HucMSCs were screened by puromycin (3 mg/mL, Solarbio Technology Co., Ltd, Beijing, China), followed by separation of EVs.

2.4. Experimental animals

Male adult Sprague Dawley rats (150–200 g) were procured from Shanghai Jihui Experimental Animal Breeding Co., Ltd. (China). All rats were raised in a laboratory at specific pathogen free level. The experiments got the approval of the Animal Care and Use Committee of The First Affiliated Hospital, Sun Yat-sen University and followed the Guide for the Care and Use of Laboratory Animals [26].

2.5. Establishment and treatment of the SCI model

After anesthetization with pentobarbital (50 mg/kg, i.p), all rats were subjected to laminectomy on bilateral T9-T11 segment [27], meaning that the T10 spinal cord was lifted with a spinal cord hook and the entire spinal cord was transected using a microsurgical scissors. Sham-operated rats underwent resection of bilateral laminae without damaging the spinal cord. After modeling, the muscle and skin were sutured in layers, and the urine was artificially discharged twice a day until the spontaneous urination was restored. At 24 h after surgery, rats were injected with EVs or GW via the caudal vein for 10 consecutive days with 50 μg dose for each injection. Lentiviruses (5×10^8 TU/mL) used to package KDM6A overexpression vector and the negative control (NC) were procured from GeneCopeia (Rockville, MD, USA) and injected into rats via the caudal vein at 24 h and on the 7th day after surgery, with the dose of 2×10^7 TU for each injection. On the 28th day after surgery, all rats underwent euthanasia by pentobarbital (200 mg/kg, i.p). The spinal cord tissue was extracted immediately, with 6 random ones in each group for tissue embedding and sectioning and the rest 6 ones in each group used for detection of tissue homogenates.

EVs were prelabeled with PHK26 (Sigma–Aldrich) and incubated in the dark at 37 °C for 15 min, followed by 60 min of centrifugation at 16,000 *g* for removal of the supernatant. After 3 washes with PBS, labeled EVs were injected into rats. The in vivo EVs were observed with the help of an Olympus BX41 microscope (Magnafire, Olympus, Tokyo, Japan) equipped with charge-coupled device.

2.6. Basso-Beattie-Bresnahan (BBB) scoring

The recovery of hind limb motor function on the 7th, 14th, 21st, and 28th d after damage was evaluated by means of BBB scoring. Rats were placed in a 125 cm × 125 cm open field for observation of animal movement after acclimatization. The animal movement was observed by the double blind method for about 5 min and was scored by two non-experimental personnel who were expert in BBB quantitative scoring. The average of the 3 recorded values was regarded as the BBB score. Generally, 0 score is indicative of complete paralysis and 21 score is indicative of normal motor.

2.7. Tissue staining

After euthanizing the animals on the 28th d after surgery, the spinal cord tissues 0.5 cm above and below the injury center of 6 rats in each group were taken for routine dehydration, paraffin embedding, and sectioning. After 2 times of xylene dewaxing (5 min/time), dehydration with gradient ethyl alcohol (5 min with 100 % ethyl alcohol, 3 min with 95 % ethyl alcohol, 3 min with 90 % ethyl alcohol), and 3 washes with running water, tissue slices were stained with hematoxylin (Beyotime Biotechnology Co., Shanghai, China). After 3 washes and 29 s differentiation with hydrochloric acid and ethyl alcohol, tissue slices were stained with 1 % eosin for 5 min. The Nissl staining was conducted through 30 min of dyeing with toluidine blue according the kit protocol (Beyotime Biotechnology Co.). After rinsing, the histological changes of spinal cord and Nissl substance were observed under an optical microscope.

2.8. Cell culture and treatment

Undifferentiated PC12 cells (ATCC, Manassas, VA, USA) were cultured in Roswell Park Memorial Institute (RPMI)-1640 medium (ATCC) containing 5 % FBS, 1 % antibiotics (Streptomycin/Penicillin), and 10 % thermally inactivated horse serum (Sigma–Aldrich) at 37 °C with 5 % CO_2 in the air. After cells were adherent to the plate, the culture medium was replaced with differentiation medium [RPMI-1640 supplemented with 50 ng/mL nerve growth factor (NGF; Sigma–Aldrich), 1 % horse serum (Sigma–Aldrich), and 1 % antibiotics]. Neuron-differentiated PC12 cells were garnered after 7 days of culture. Differentiated PC12 cells were used for the subsequent assays.

PC12 cells were stimulated with increasing doses of lipopolysaccharide (LPS; 0, 1, 2, 5, 10 μg/mL; Sigma–Aldrich) for 12 h. PC12 cells treated with 5 μg/mL LPS were used to simulate in vitro nerve injury model, with cells treated with an equal volume of PBS (Sigma–Aldrich) as the control. Cells were differentiated before subsequent experimentation. As for EVs treatment, PC12 cells were incubated with 50 μg/mL EVs, with cells incorporated with an equal volume of GW4869-treated conditioned medium as the control group. Cells were incubated for 24 h before the subsequent tests. As for genetic intervention, PC12 cells were transfected with KDM6A pcDNA3.1, NOX4 pcDNA3.1, and the empty vector (RiboBio, China) using Lipofectamine 2000 (Invitrogen, USA) following the protocol. Transfected cells were treated with LPS for further analysis.

2.9. Observation of EVs endocytosis

To monitor EVs-mediated delivery of miR-26b-5p, Cy3-miR-26b-5p mimic (GenePharma, Shanghai, China) was transfected into HucMSCs using Lipofectamine 2000. After 6 h of transfection, HucMSCs were cocultured with PC12 cells [green fluorescent protein (GFP) green fluorescence] at the 24-well Transwell chamber for 48 h. In addition, GW4869 was incorporated into the above system, which was named as the EVs release inhibition group. Eventually, the delivery of miR-26b-5p was monitored by a confocal microscopy (LSM710, Carl Zeiss, Jena, Germany).

2.10. Cell counting kit-8 (CCK-8) assay

PC12 cells were cultured at the 96-well plate overnight and underwent designated transfection. After 48 h, cells were exposed to 5 μg/mL LPS for 12 h, followed by 3 h of incubation with 10 μL CCK-8 reagent (Beyotime Biotechnology Co.). At last, cell viability was calculated by measurement of optical density at a wavelength of 450 nm.

2.11. ROS assay

ROS levels in tissues ($n = 6$) and cells were determined using dihydroethidium (DHE) staining (Beyotime) or 2,7-dichlorofluorescein diacetate (DCFDA; Beyotime). Spinal cord slices were treated with 5 μm DHE reagent and incubated in a humidified darkroom at 37 °C for 30 min. Cells were incubated with 50 μM DCFDA for 45 min, followed by removal of DCFDA and 2 washes with PBS (pH 7.4). The fluorescence intensity of DCFDA was determined using a fluorescence spectrophotometer (Synergy MX, BioTek, Winooski, VT, USA) at an excitation wavelength of 485 nm and an emission wavelength of 538 nm.

2.12. Terminal deoxynucleotidyl transferase-mediated dUTP-biotin nick end labeling (TUNEL) staining

Apoptosis was detected using the TUNEL assay kit (Roche, Mannheim, Germany). Apoptosis rate was presented as positive staining cell number/total cell number × 100 %. Stained cells were analyzed using a Nikon ECLIPSE Ti microscope (Nikon, Tokyo, Japan).

2.13. Enzyme-linked immunosorbent assay (ELISA)

According to the producer's instructions, the levels of tumor necrosis factor-α (TNF-α; ab236721, Abcam), interleukin (IL)-6 (MBS2885203, MyBiosource, San Diego, CA, USA), and IL-1β (MBS2023030, MyBiosource) in tissues (n = 6) and cells were determined using corresponding commercially available ELISA kits.

2.14. Quantitative real-time polymerase chain reaction (qRT-PCR)

The total RNA was prepared from an equal quantity of cells (5×10^5) and tissues (n = 6) using the TRIzol reagent (Invitrogen). The Total Exosome RNA&Protein Separation kit (Invitrogen) was used to separate RNA from equal amounts of EVs. RNA quantification was performed using a microplate reader (Bio-Tek). RNA samples were reverse-transcribed into the complementary DNA using the PrimeScript RT reagent kit (Takara, Tokyo, Japan). Next, qRT-PCR analysis was conducted with the use of SYBR™Green PCR Master Mix (Thermo Fisher Scientific) and primers (Table 1). With glyceraldehyde-3-phosphate dehydrogenase (GAPDH) or U6 [28] or miR-22-5p [29] as the internal control, the fold changes were determined according to the $2^{-\Delta\Delta Ct}$ method [30].

2.15. Western blot assay

Tissues (n = 6) and cells (5×10^5) were lysed using radioimmunoprecipitation assay lysis buffer containing proteinase inhibitor (Beyotime). Protein concentrations in lysates were quantified using the bicinchoninic acid reagent. An equal amount of protein was separated on 7.5–12.5 % sodium dodecyl sulfate polyacrylamide gel electrophoresis and transferred onto polyvinylidene fluoride membranes (Bio-Rad, Hercules, CA, USA). After a blockade with 5 % skim milk in Tris buffered saline Tween (TBST) at room temperature for 2 h, incubation was conducted on membranes with primary antibodies against KDM6A (1:2000, ab36938, Abcam), NOX4 (1:1000, ab154244, Abcam), and β-actin (1:2000, ab8227, Abcam) at 4 °C overnight. After washing with TBST, the membranes underwent 1 h of incubation with horseradish peroxidase-coupled secondary antibody against immunoglobulin G (1:5000, ab6721, Abcam) at room temperature. Eventually, signals underwent visualization with ChemiDicTM XRS + ImagingSystem (Bio-Rad) and quantitative analysis with Image Lab.

Table 1
PCR primer sequences.

Name	Sequence (5′-3′)
miR-26b-5p	F: TCGGCAGGTTCAAGTAATTCA
	R: CTCAACTGGTGTCGTGGA
KDM6A	F: AATCCTGCGGAGTGTCGCTCGCTAC
	R: CCGAAAAGGCGGCTGTCCAGTCCAC
NOX4	F: GGCTGGCCAACGAAGGGGTTAAAC
	R: CAGGCTGCAGTTGAGGTTCAGGAC
miR-22-5p	F: GCCGAGAGTTCTTCAGTGGCA
	R: CTCAACTGGTGTCGTGGA
U6	F: TCGCTTCGGCAGCACATATACT
	R: AGGTGGCTTTGGTGGAAGAG
GAPDH	F: GGTCCCAGCTTAGGTTCATCA
	R: AATCCGTTCACACCGACCTT
NOX4 promoter	F: GGAAGCTATGCTCAGTTCCCATC
	R: AGGTTTGCTCCTCCAAACCTAGAG

2.16. Dual-luciferase assay

KDM6A 3′UTR fragments containing the bindings site with miR-26b-5p and the mutant sequence at the target site were amplified and inserted into pmirGLO reporter luciferase vector (Promega), resulting in wild type and mutant type of reporter vectors (KDM6A-WT and KDM6A-MUT). Next, PC12 cells were seeded into the 24-well plates and co-transfected with the constructed luciferase vectors and miR-26b-5p mimic or miR-NC. After 48 h, the luciferase activity was analyzed with the help of the dual-luciferase® reporter gene analysis system (Promega).

2.17. Chromatin immunoprecipitation (ChIP) analysis

The enrichment of KDM6A and H3K27me3 at the NOX4 promoter was determined by ChIP assay dependent on the EZ-Magna ChIP A/G assay kit (Millipore, Bedford, MA, USA). Cells were crosslinked with 1 % formaldehyde and quenched with glycine, followed by ultrasound treatment. The supernatant was mixed with Magna ChIP Protein A/G magnetic beads that were precoupled with antibodies against KDM6A (1:2000, ab36938, Abcam), H3K27me3 (1:2000, ab192985, Abcam) and IgG (1:2000, ab171870, Abcam) at 4 °C. Subsequently, the immunoprecipitated complex was collected, washed, and eluted. After these steps, the complex was incubated with proteinase K at 65 °C for 2 h and further incubated at 95 °C for 15 min for reversing crosslink and removing proteins. The eluted DNA serve as the template for qPCR analysis. The primers are enlisted in Table 1.

2.18. Statistical analysis

Statistical analysis and plotting of data were executed using SPSS21.0 statistical software (IBM SPSS Statistics, Chicago, IL, USA) and GraphPad Prism 8.0 software (GraphPad Software Inc., San Diego, CA, USA). First, data were tested by normality and homogeneity of variance assays, that data were in normal distribution and homogeneity of variance. Pairwise comparisons of data were conducted by the *t* test, and multigroup comparisons of data were conducted by one-way or two-way analysis of variance (ANOVA), followed by Tukey's multiple comparison test used for post-hoc testing. $P < 0.05$ was indicative of statistical significance and $P < 0.01$ was considered extremely statistical significance.

3. Results

3.1. Separation and culture of HucMSCs, and extraction and identification of HucMSCs-EVs

HucMSCs were separated and cultured (Fig. 1A). Flow cytometry showed that surface antigens CD73 and CD90 were positive while CD31 and CD34 were negative (Fig. 1B). Meanwhile, HucMSCs presented with great potentials for osteogenic and adipogenic differentiation (Fig. 1C), suggesting the successful separation of HucMSCs. Thereafter, EVs were separated from HucMSCs and presented with circle or oval in shape and integrity of membrane structure, which was the classical morphology of EVs (Fig. 1D). NTA analysis revealed a particle diameter of 30~150 nm range (Fig. 1E). Western blot assay revealed that CD63 and CD9 were expressed in EVs while Calnexin was not expressed in EVs (Fig. 1F). The above results suggested that HucMSCs-derived EVs were successfully separated.

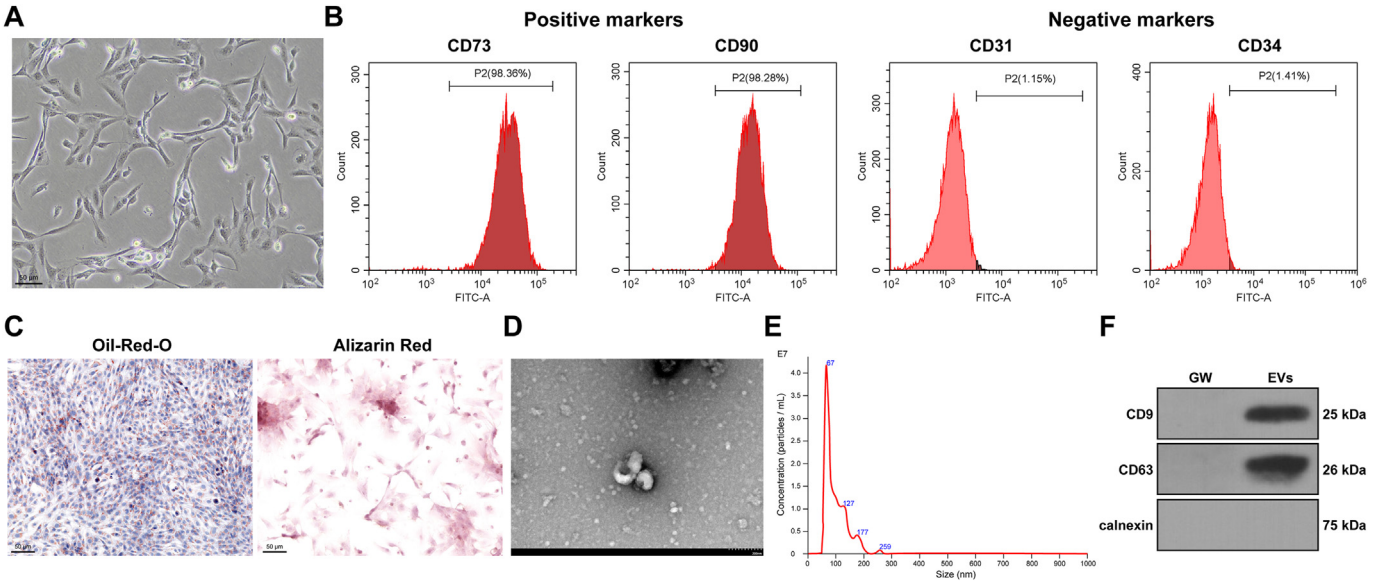

Fig. 1. Separation, culture of HucMSCs and extraction, identification of HucMSCs-EVs. A: HucMSCs were observed by optical microscopy; B: HucMSCs surface antigens CD73, CD90, CD31, CD34 were determined by flow cytometry; C: Osteogenic and adipogenic differentiation of HucMSCs was observed by oil red O staining and alizarin red staining; D: EVs were observed by transmission electron microscopy; E: Particle size and concentration of EVs were analyzed by a nanoparticle tracking analyzer; F: Expression levels of CD63, CD9, and Calnexin were determined by Western blot assay. Experiments were repeated 3 times independently. GW: GW4869-treated conditioned medium of HucMSCs.

3.2. HucMSCs-EVs alleviates the injury of SCI mice

First, the SCI rat model was established. A series of evaluations of SCI rats revealed that the BBB score of SCI rats was significantly decreased ($P < 0.01$, Fig. 2A); the structure of spinal cord was impaired gradually with presence of cavity (Fig. 2B); the positive rate of TUNEL int tissues was increased ($P < 0.01$, Fig. 2C); the ROS content was elevated ($P < 0.01$, Fig. 2D), and the levels of inflammatory cytokines TNF-α, IL-1β, and IL-6 were notably augmented ($P < 0.01$, Fig. 2E). After injection of EVs, SCI rats presented with significantly functional recovery ($P < 0.01$, Fig. 2A–E), and the spinal cord was observed with PKH26 labelled fluorescence of EVs (Fig. 2F). The above results provided evidence that HucMSCs-EVs was beneficial for alleviation of injury in SCI rats.

3.3. HucMSCs-EVs alleviate LPS-induced cell injury and inflammation in vitro

Meanwhile, the cell injury model was established in vitro. LPS treatment brought about reduced cell viability ($P < 0.01$, Fig. 3A) and elevated cell apoptosis ($P < 0.01$, Fig. 3B), ROS content ($P < 0.01$, Fig. 3C), and levels of TNF-α, IL-1β, and IL-6 ($P < 0.01$, Fig. 3D). Relative to LPS treatment, EVs treatment contributed to enhancing cell viability ($P < 0.01$, Fig. 3A) and reducing in cell apoptosis ($P < 0.01$, Fig. 3B), ROS content ($P < 0.01$, Fig. 3C), and levels of TNF-α, IL-1β, and IL-6 ($P < 0.01$, Fig. 3D), while GW treatment had not above effects, suggesting that HucMSCs-EVs alleviated LPS-induced cell injury and inflammation in vitro.

3.4. HucMSCs-EVs deliver miR-26b-5p into neurons

HucMSCs-EVs may mediate the transport of EVs to facilitate the recovery from SCI [31], and the downregulation of miR-26b has been documented in SCI [17]. We conjectured that EVs may play a role in SCI through delivery of miR-26b-5p. Extracted EVs were treated with Rnase I, which revealed no change in miR-26b-5p expression, while the combined treatment of Rnase I and Triton X-100 obviously reduced the expression of miR-26b-5p in EVs ($P < 0.01$, Fig. 4A), suggesting that miR-26b-5p was enveloped in EVs. In addition, miR-26b-5p was found to be weakly expressed in in vivo and in vitro SCI models and upregulated in response to EVs treatment ($P < 0.01$, Fig. 4B). Taking advantage of Cy3 labeling, a large amount of red fluorescence was observed in PC12 cells after co-culture of HucMSCs and PC12 cells, while the red fluorescence disappeared under the role of GW4869 (Fig. 4C).

Next, miR-26b-5p was overexpressed in HucMSCs ($P < 0.01$, Fig. 4D), followed by separation of EVs-26b-5p, which revealed the marked upregulation of miR-26b-5p in EVs-26b-5p ($P < 0.01$, Fig. 4D). Subsequently, EVs-26b-5p was used for in vivo and in vitro assays, which revealed that it exerted better alleviative effects for SCI both in vivo and in vitro ($P < 0.01$, Fig. 4E-M). In conclusion, HucMSCs-EVs may mediate the delivery of miR-26b-5p into spinal cord tissues and cells, thus alleviating SCI.

3.5. miR-26b-5p targets the inhibition of KDM6A, and KDM6A promotes NOX4 expression through histone demethylation

Epigenetic alteration is one of mechanisms that induce and maintain neuropathic pain, and H3K27me2/3 is an inhibitory biomarker that induces chromatin compaction thereby causing gene inactivation [18]. KDM6A has been reported to be upregulated in SCI and inhibit H3K27me3 levels [22]. The targeted binding relationship between miR-26b-5p and KDM6A 3′UTR (Fig. 5A) was predicted through TargetScan online analysis, which was further verified by the dual-luciferase assay ($P < 0.01$, Fig. 5B). qRT-PCR and Western blot assays revealed that KDM6A was highly expressed in both in vivo and in vitro SCI models and was significantly downregulated under the role of EVs treatment ($P < 0.01$, Fig. 5C, E), suggesting that EVs-mediated delivery of miR-26b-5p into cells repressed KDM6A expression.

NOX4 plays a role in the induction of oxidative stress after SCI [24,25]. In ChIP assay, KDM6A was found to have significant enrichment at the NOX4 promoter in model tissues and cells, and such enrichment was relatively reduced while the enrichment of H3K27me3 was relatively elevated after EVs treatment ($P < 0.01$, Fig. 5D). qRT-PCR and Western blot assays disclosed that NOX4

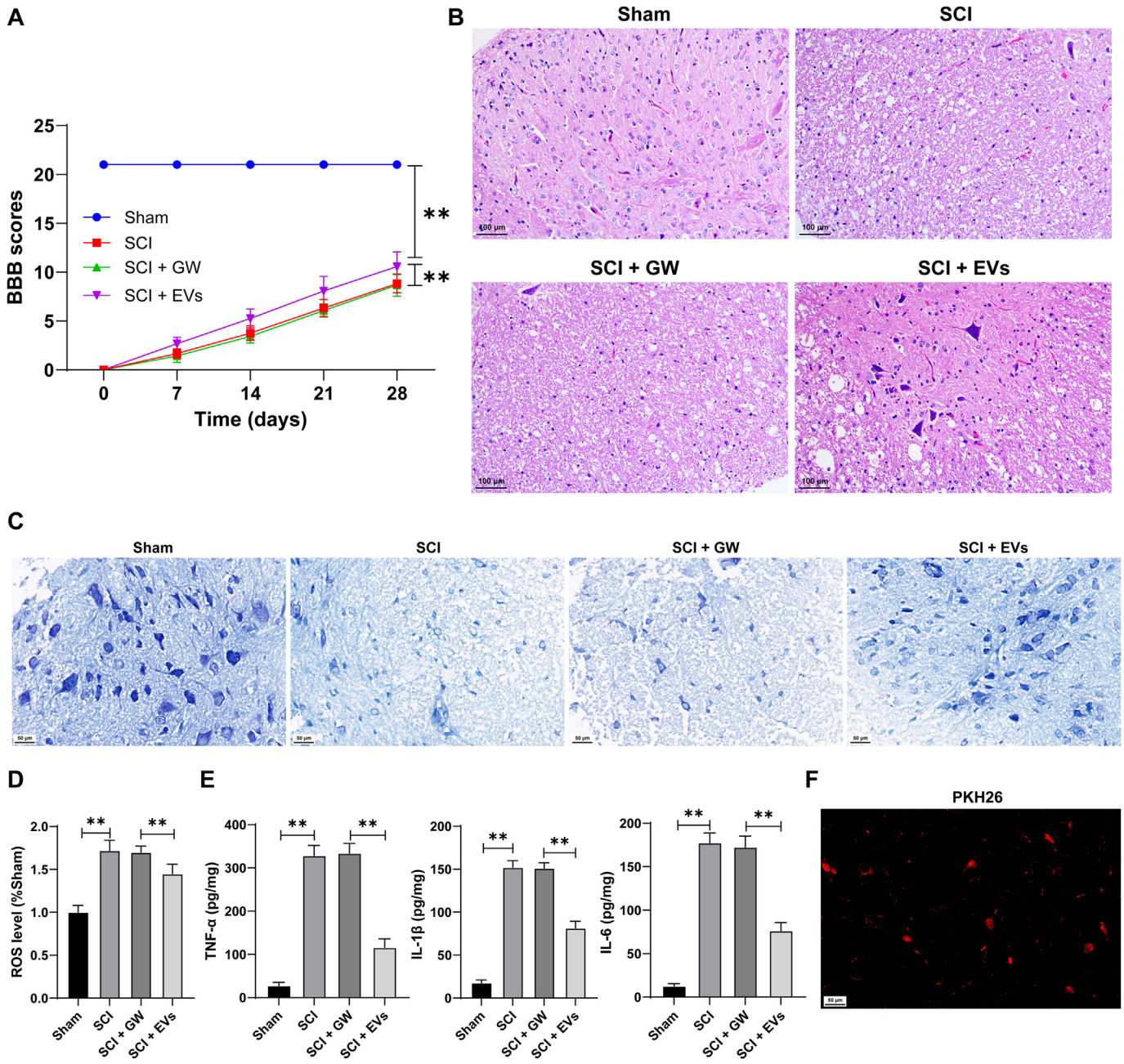

Fig. 2. HucMSCs-EVs alleviates the injury of SCI mice. The SCI rat model was established and SCI rats were injected with EVs or GW at 24 h after surgery for 10 consecutive days. A: BBB scoring was performed on the 0th, 7th, 14th, 21st, and 28th d after surgery, n = 12; B: Pathological changes of spinal cord were observed by H&E staining, n = 6; C: Cell apoptosis was evaluated by TUNEL staining, n = 6; D: ROS levels were determined by dihydroethidium staining, n = 6; E: Levels of TNF-α, IL-1β, and IL-6 in tissues were determined by ELISA, n = 6; F: PHK26-labelled EVs were injected into SCI rats and observed by fluorescence microscopy. $^{**}P < 0.01$. Data A were analyzed by two-way ANOVA, and data C and D were analyzed by one-way ANOVA, followed by Tukey's multiple comparison test.

expression was upregulated in SCI model group while was reduced in response to EVs treatment ($P < 0.01$, Fig. 5C, E), suggesting that KDM6A may promote NOX4 expression by erasing H3K27me3 occupation.

3.6. KDM6A overexpression reverses the alleviative role of EVs-26b-5p in LPS-induced cell injury

KDM6A was overexpressed in PC12 cells ($P < 0.01$, Fig. 6A and B), followed by combined treatment with EVs-26b-5p to confirm the above mechanism. Our results revealed that relative to EVs-26b-5p treatment alone, KDM6A overexpression brought about elevated NOX4 expression in PC12 cells ($P < 0.01$, Fig. 6A and B), reduced cell viability ($P < 0.01$, Fig. 6C), intensified cell apoptosis ($P < 0.01$, Fig. 6D), and increased in ROS content ($P < 0.01$, Fig. 6E) and levels of TNF-α, IL-1β, and IL-6 ($P < 0.01$, Fig. 6F), suggesting that KDM6A overexpression reversed the alleviative role of EVs-26b-5p in LPS-induced cell injury.

3.7. NOX4 overexpression reverses the alleviative role of EVs-26b-5p in LPS-induced cell injury

Next, NOX4 was overexpressed in PC12 cells ($P < 0.01$, Fig. 7A and B), followed by combined treatment with EVs-26b-5p to

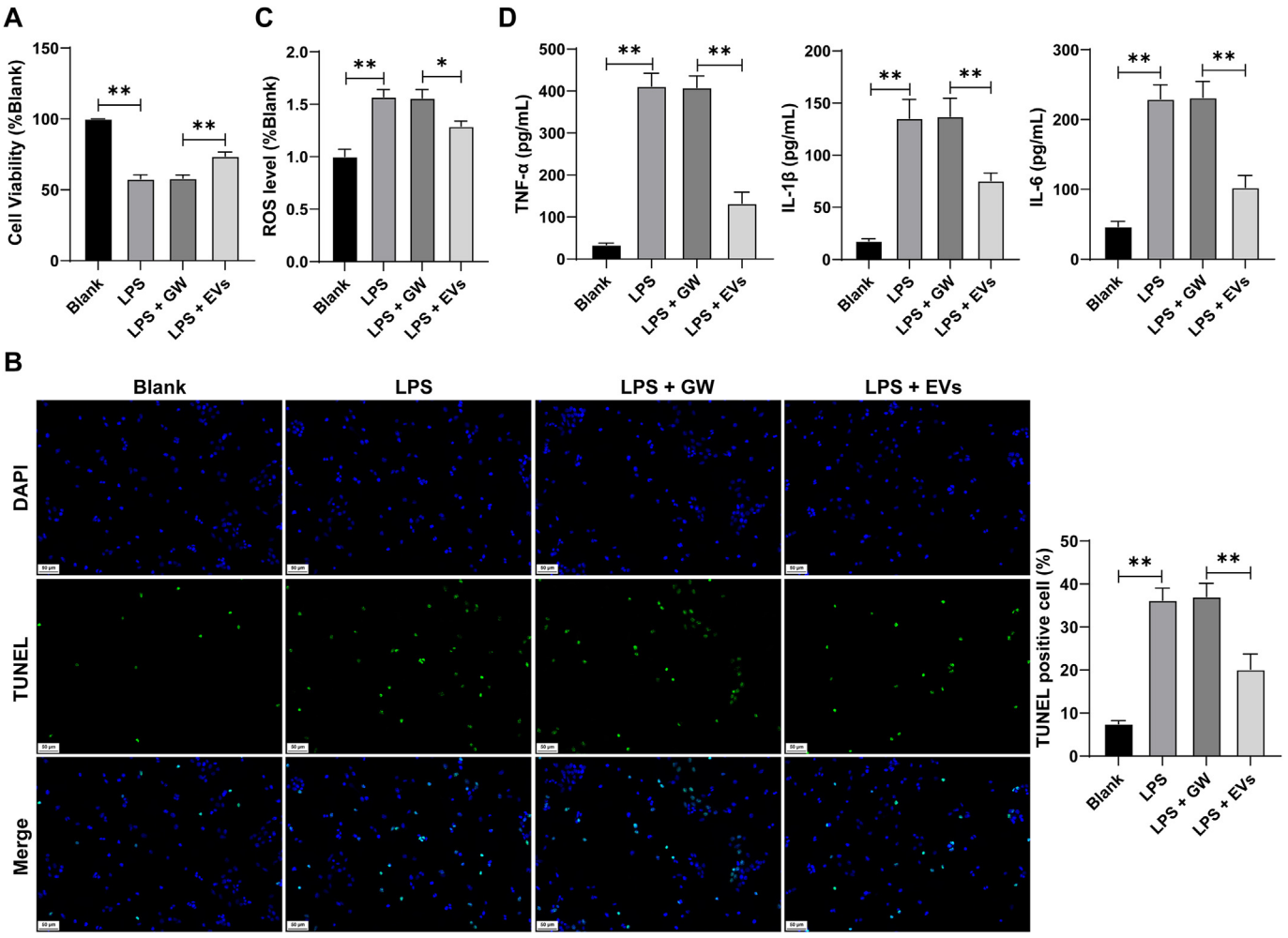

Fig. 3. HucMSCs-EVs alleviate LPS-induced cell injury and inflammation in vitro. PC12 cells were incubated with 50 μg/mL EVs or GW, and 5 μg/mL LPS was used to stimulate cells for 12 h. A: Cell viability was examined by CCK-8 assay; B: Cell apoptosis was observed by TUNEL staining; C: ROS content was determined by 2,7-dichlorofluorescein diacetate staining; D: Levels of TNF-α, IL-1β, and IL-6 in cells were determined by ELISA. Cell experiments were repeated 3 times independently. *$P < 0.05$, **$P < 0.01$. Data were analyzed by one-way ANOVA, followed by Tukey's multiple comparison test.

confirm the functionality of NOX4 in the whole mechanism of SCI. Our results showed that relative to EVs-26b-5p treatment alone, NOX4 overexpression reduced cell viability ($P < 0.01$, Fig. 7C), enhanced cell apoptosis ($P < 0.01$, Fig. 7D), elevated ROS content ($P < 0.01$, Fig. 7E), and augmented the levels of TNF-α, IL-1β, and IL-6 ($P < 0.01$, Fig. 7F), indicating that NOX4 overexpression reverse the alleviative role of EVs-26b-5p in LPS-induced cell injury.

3.8. KDM6A reverses the alleviative role of EVs-26b-5p in SCI in vivo

Eventually, the expression of KDM6A was upregulated in vivo ($P < 0.01$, Fig. 8A and B), followed by combined treatment with EVs-26b-5p. Our results showed that after KDM6A overexpression, the expression of NOX4 was elevated in the spinal cord ($P < 0.01$, Fig. 8A and B); BBB score was reduced ($P < 0.01$, Fig. 8C); the pathological changes of the spinal cord were exacerbated ($P < 0.01$, Fig. 8D); the number of TUNEL-positive cells was augmented ($P < 0.01$, Fig. 8E); and the levels of ROS, TNF-α, IL-1β, and IL-6 were increased in tissues ($P < 0.01$, Fig. 8F and G). Altogether, our results elucidated that KDM6A reversed the alleviative role of EVs-26b-5p in SCI in vivo.

4. Discussion

Spinal cord injury (SCI) is a neurological trauma with high disability rate, resulting in multiple adverse neurological events, such as neuronal apoptosis, neuroinflammation, and ROS production [1]. Currently, there is a lack of effective therapies to improve the functional recovery after SCI. Fortunately, MSCs and MSCs-EVs have provided new hope for the management of SCI, and MSCs-EVs should be utilized more in the clinical setting due to higher safety and more efficient delivery of therapeutic substances to recipient cells relative to MSCs [8]. In this paper, our data suggested that HucMSCs-EVs improved neurological recovery post SCI by carrying miR-26b-5p to target the intracellular KDM6A/NOX4 axis, and this effect was enhanced after overexpression of miR-26b-5p in EVs (Fig. 9).

Different stem cells, such as neural stem cells, MSCs, and embryonic stem cells exert differential therapeutic functions in SCI. EVs from MSCs are gaining more attraction as an alternative to cell-based therapies by virtue of the less ethical issues involved, as well as their advantages of easier acquisition, preservation, sterilization, and packaging [32]. By acting through the paracrine mechanism, MSCs-EVs can exert neuroprotection after SCI while overcoming some side effects of MSCs therapy. Intravenous infusion of MSCs

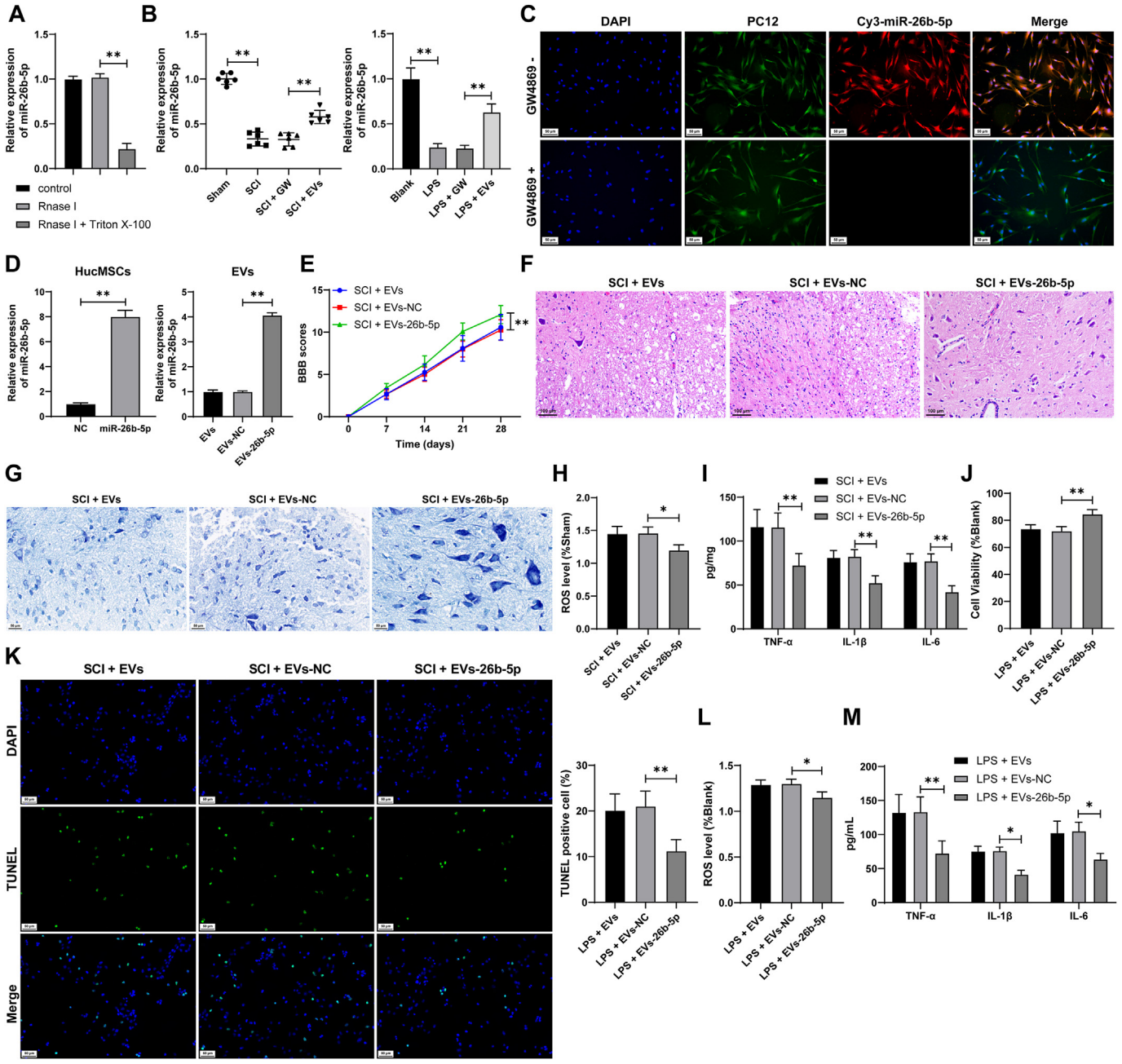

Fig. 4. HucMSCs-EVs deliver miR-26b-5p into spinal cord tissue and cells to alleviate SCI. A: Extracted EVs were treated with Rnase I or Triton X-100, and miR-26b-5p expression was determined by qRT-PCR; B: miR-26b-5p expression levels were measured by qPCR in spinal cord tissues of sham, SCI, SCI + GW, and SCI + EVs groups; C: miR-26b-5p was labeled by Cy3 in HucMSCs, and HucMSCs were cocultured with GFP-labeled PC12 cells under the condition of GW4869 or no GW4869 to observe the fluorescence; miR-26b-5p was overexpressed in HucMSCs, followed by extraction of EVs; D: miR-26b-5p expression in HucMSCs and EVs was determined by qRT-PCR; SCI rats and LPS-treated PC12 cells were treated with the above EVs; E: BBB scoring, n = 12; F: Pathological changes of spinal cord were observed by H&E staining, n = 6; G: Cell apoptosis was evaluated by TUNEL staining, n = 6; H: ROS levels were determined by dihydroethidium staining, n = 6; I: Levels of TNF-α, IL-1β, and IL-6 in tissues were determined by ELISA, n = 6; J: Cell viability was examined by CCK-8 assay; K: Cell apoptosis was observed by TUNEL staining; L: ROS content was determined by 2,7-dichlorofluorescein diacetate staining; M: Levels of TNF-α, IL-1β, and IL-6 in cells were determined by ELISA. Cell experiments were repeated 3 times independently. *$P < 0.05$, **$P < 0.01$. Data A, B, D (right), G, H, J, K, L were analyzed by one-way ANOVA, and data E, I, and M were analyzed by two-way ANOVA, followed by Tukey's multiple comparison test. Data D (left) were analyzed by the *t* test.

can secrete EVs that are trafficked to the injury site, thus promoting M2 polarization of macrophages, reducing the blood-spinal cord barrier, and improving functional recovery after SCI [33]. Moreover, pretreated MSCs-EVs like melatonin-preconditioned MSCs-EVs and hypoxic preconditioned MSCs-EVs may better benefit the neurological outcome by orchestrating microglia/macrophages polarization [11,34]. According to our results, injection of MSCs-EVs into SCI model rats improved the motor function and the integrity of spinal cord, while reduced neuronal apoptosis and release of inflammatory factors. In vitro, MSCs-EVs exert antiapoptotic, anti-inflammatory, and antioxidative effects in LPS-induced SCI cell model.

miRNAs are the most abundant RNAs shuttled by EVs and represent the most important therapeutic substances for SCI [35]. Numerous MSC-derived exosomal miRNAs have been reported to participate in pathophysiological processes of SCI by regulating the

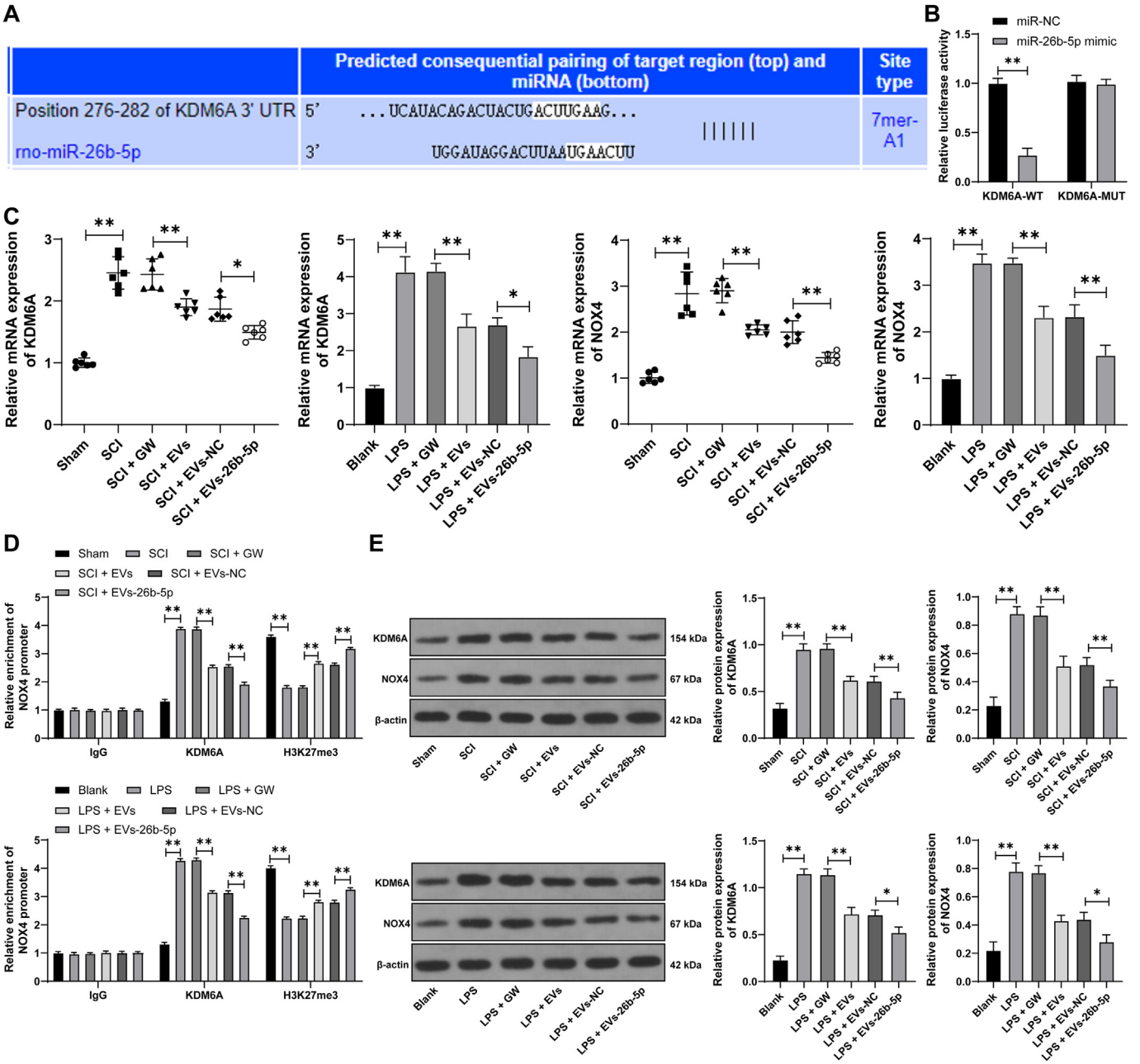

Fig. 5. miR-26b-5p targets the inhibition of KDM6A, and KDM6A promotes NOX4 expression through histone demethylation. A: The binding site between miR-26b-5p and KDM6A 3′UTR was analyzed online by the TargetScan database; B: The binding relationship between miR-26b-5p and KDM6A 3′UTR was verified by the dual-luciferase assay; C: Transcriptional levels of KDM6A and NOX4 in tissues and cells were determined by qRT-PCR; D: Enrichment of KDM6A and H3K27me3 at the NOX4 promoter; E: Protein levels of KDM6A and NOX4 in tissues and cells were determined by Western blot assay. Animal experiments, n = 6. Cell experiments were repeated 3 times independently. $^{*}P < 0.05$, $^{**}P < 0.01$. Data B and D were analyzed by two-way ANOVA and data C and E were analyzed by one-way ANOVA, followed by Tukey's multiple comparison test.

inflammatory response, neuronal death, and neural functional repair [36]. For instance, MSCs-EVs are shown to deliver miR-216a-5p and miR-124-3p to attenuate neurological damage caused by SCI [11,37]. EVs from miR-25-overexpressed-MSCs exert neuroprotective effects in an ischemic SCI model [38]. miR-126-modified MSC-EVs promote angiogenesis and neurogenesis and reduce apoptosis post SCI in rats [39]. On a separate note, miR-26b is reported be weakly expressed in the spinal cord of transgenic mice with amyotrophic lateral sclerosis [40]. Additionally, miR-26b is able to attenuate microglial activation, inflammation, and neurotoxicity in the context of neurodegenerative and cerebrovascular diseases [41]. Most significantly, a pioneering investigation has reported that miR-26b is expressed a low level in SCI and expedites the generation of myelinating oligodendrocytes leading to remyelination [17]. In the present study, we focus on miR-26b-5p since there are currently few reports regarding the role of miR-26b-5p in SCI. Our experimentation suggested that miR-26b-5p was poorly expressed in the SCI rat and cell models and MSCs-EVs transported miR-26b-5p into spinal cord-resident neurons, leading to the recovery of SCI model rats and repairment of SCI model cells. Collectively, our results demonstrated that miR-26b-5p is enveloped in the EVs secreted by MSCs-EVs, which leads to the improvement of functional recovery post SCI when transported to the injured site.

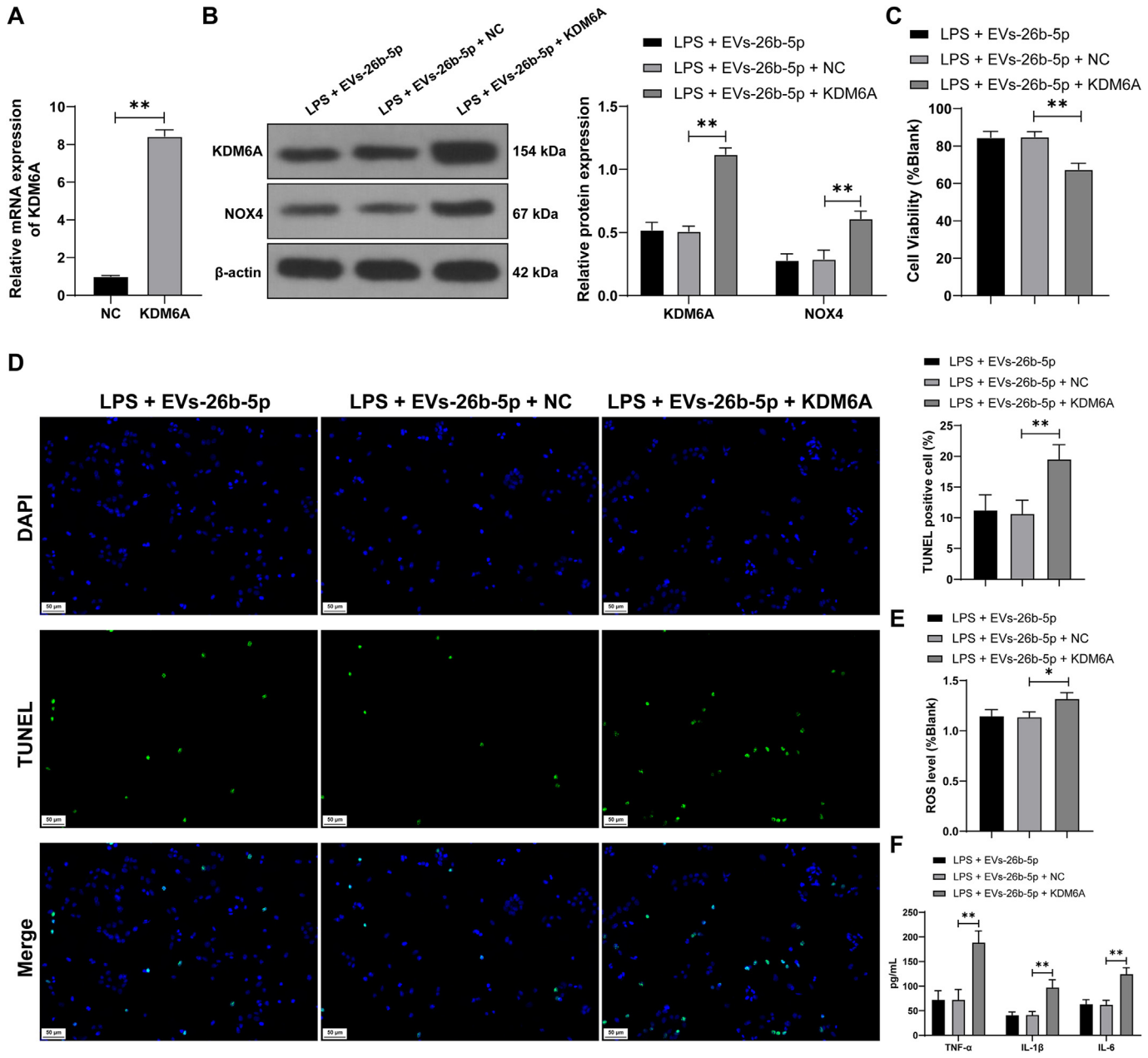

Fig. 6. KDM6A overexpression reverses the alleviative role of EVs-26b-5p in LPS-induced cell injury. PC12 cells were transfected with KDM6A pcDNA3.1 (KDM6A) to overexpress KDM6A, with cells transfected with empty vector (NC) as the control. A: Overexpression effectiveness of vectors was determined by qRT-PCR; Transfected cells were treated with EVs-26b-5p; B: Protein levels of KDM6A and NOX4 were determined by Western blot assay; C: Cell viability was evaluated by CCK-8 assay; D: Cell apoptosis was observed by TUNEL staining; E: ROS content was determined by 2,7-dichlorofluorescein diacetate staining; F: Levels of TNF-α, IL-1β, and IL-6 in cells were determined by ELISA. Cell experiments were repeated 3 times independently. $^{*}P < 0.05$, $^{**}P < 0.01$. Data A were analyzed by the *t* test, data B and F were analyzed by two-way ANOVA, and data C, D, and E were analyzed by one-way ANOVA, followed by Tukey's multiple comparison test.

KDM6A is a vital histone demethylase that controls gene expression by the epigenetic regulation of H3K27 methylation and functions in various neuropathological processes [42]. KDM6A is highly expressed in spinal cord tissues of SCI rats and LPS-induced PC12 cells. Knockdown of KDM6A protects PC12 cells from LPS-induced cell damage and expedites neurological functional recovery of SCI rats [22]. Ablation of KDM6A promotes the functional recovery of SCI mice by epigenetically triggering intrinsic neural regeneration [21]. KDM6A can significantly decrease the level of methylation in the miR-24 promoter and KDM6A deletion can epigenetically promote the vascular regeneration and functional recovery post SCI by forming a regulatory network with miR-24 [20]. In relation to this, miR-26-5p has been elucidated to mediate the negative regulation of KDM6A in vascular smooth muscle cells [43]. The binding relationship between miR-26b-5p and KDM6A was testified by the dual-luciferase assay and KDM6A expression levels were found to be increased in both in vivo and in vitro models while reduced after EVs treatment, suggesting that EVs deliver miR-26b-5p into cells to inhibit KDM6A expression. NOX4 is a vital member of NADPH oxidases enzyme family responsible for synthesis of ROS in various pathologies [44]. Although NADPH oxidases are oxidative stress markers independent of inflammatory state, the peak of NOX2 and NOX4 is associated with microglial/macrophage polarization towards the M1

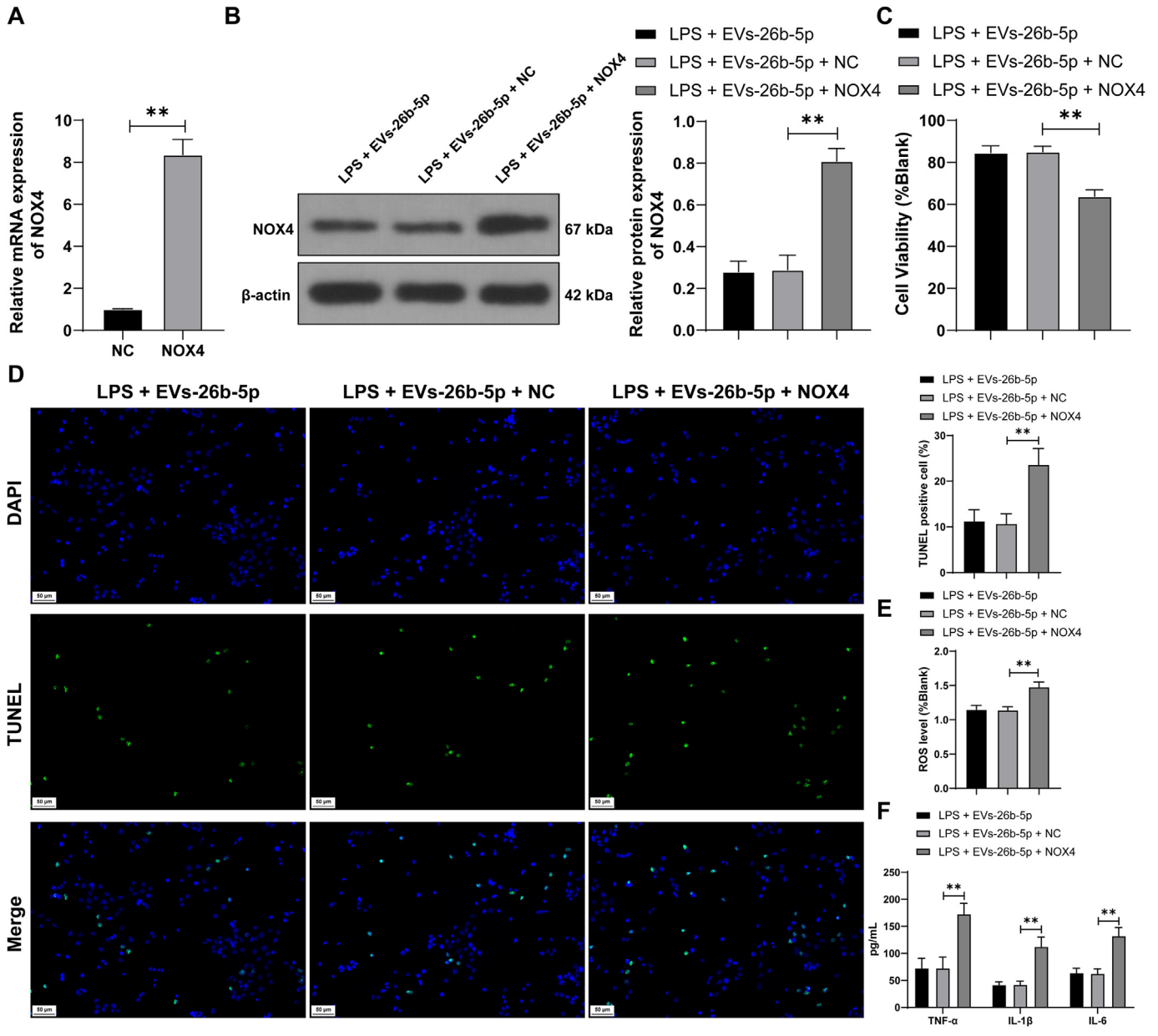

Fig. 7. NOX4 overexpression reverses the alleviative role of HucMSCs-EVs in LPS-induced cell injury. PC12 cells were transfected with NOX4 pcDNA3.1 (NOX4) to overexpress NOX4, with cells transfected with empty vector (NC) as the control. A: Overexpression effectiveness of vectors was determined by qRT-PCR; Transfected cells were treated with EVs-26b-5p; B: Protein levels of NOX4 were determined by Western blot assay; C: Cell viability was evaluated by CCK-8 assay; D: Cell apoptosis was observed by TUNEL staining; E: ROS content was determined by 2,7-dichlorofluorescein diacetate staining; F: Levels of TNF-α, IL-1β, and IL-6 in cells were determined by ELISA. Cell experiments were repeated 3 times independently. $^{*}P < 0.05$, $^{**}P < 0.01$. Data A were analyzed by the *t* test, data B and F were analyzed by two-way ANOVA, and data C, D, and E were analyzed by one-way ANOVA, followed by Tukey's multiple comparison test.

phenotype after SCI [45]. More significantly, the transcription of NOX4 tends to be altered under the role of histone methylation mechanism [46,47]. In our experiments, a large amount of KDM6A enrichment was found at the NOX4 promoter, while EVs treatment reduced KDM6A enrichment and increased H3K27me3 enrichment at the NOX4 promoter by repressing KDM6A expression. Therefore, it is plausible that KDM6A may promote NOX4 expression by erasing H3K27me3 at the NOX4 promoter. Subsequently, KDM6A and NOX4 were overexpressed in SCI model cells treated with EVs, which resulted in intensified apoptosis, oxidative stress, and inflammatory responses. Moreover, the in vivo assay further verified that KDM6A overexpression counteracted the alleviative role of EVs-26b-5p in SCI model rats.

However, there are a few limitations in the study to be resolved. First, EVs can carry plenty of small molecules and there are also many miRNAs involved in SCI pathology, and the roles and regulatory mechanisms of other miRNAs in SCI are also part of our future research project. Second, miR-26b-5p has many downstream target genes, but we only verified the role of the miR-26b-5p/H3K27me3/NOX4 axis in SCI. Third, our manuscript currently does not explore the differentiation of oligodendrocytes during SCI, so whether the role of EVs is related to oligodendrocytes still needs to be demonstrated through relevant experiments in the future. Last but not least, our experiments are still in the preclinical stage and further efforts are needed to promote the clinical transition of our findings. Going forward, we shall explore other

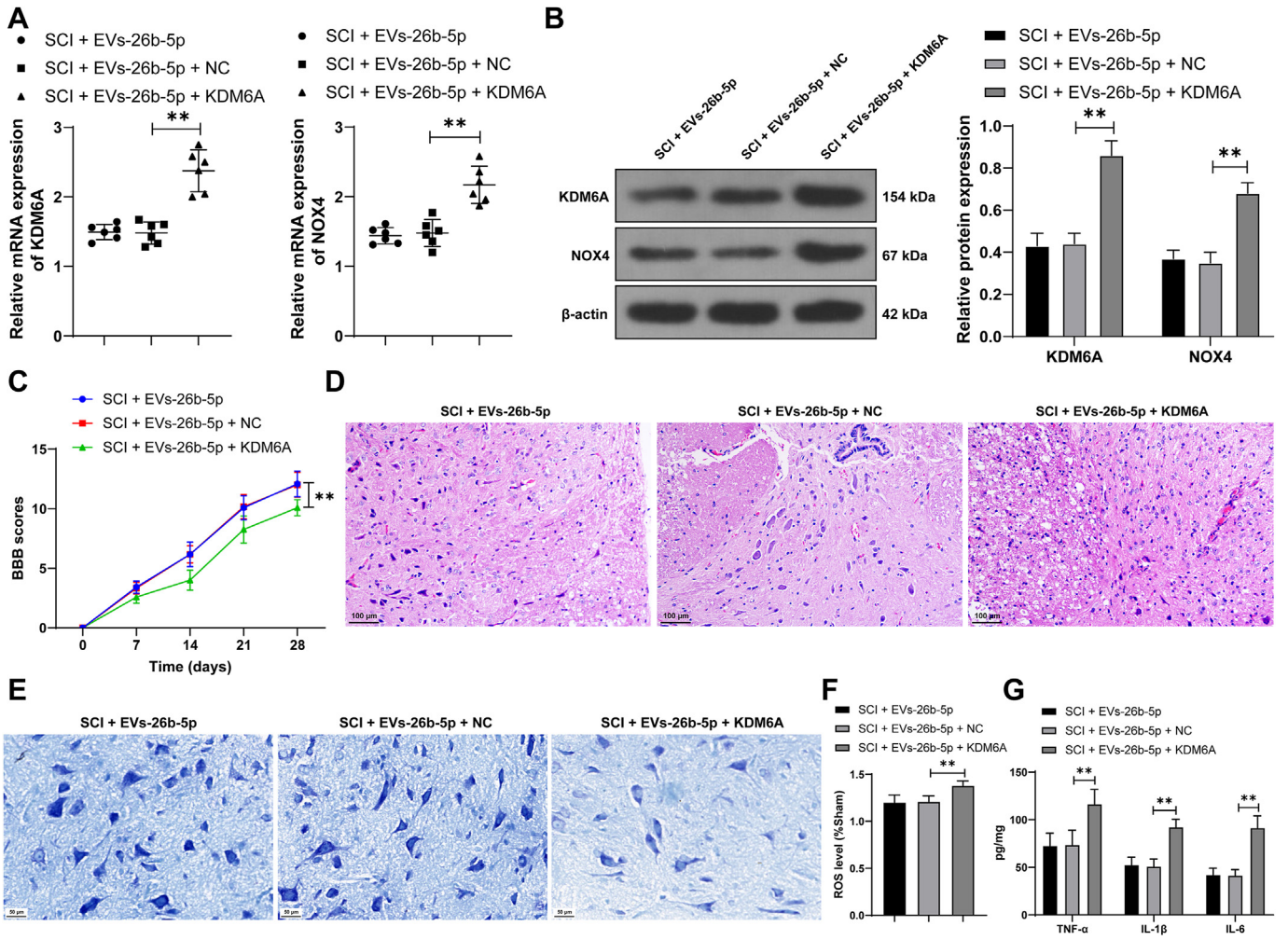

Fig. 8. KDM6A reverses the alleviative role of EVs-26b-5p in SCI in vivo. Rats were injected with adenovirus-packaged KDM6A overexpression vector (KDM6A) via the caudal vein after SCI surgery, with empty vector (NC) as the control. A–B: Expression levels of KDM6A and NOX4 in the spinal cord were determined by qRT-PCR and Western blot assay, n = 6; C: BBB scoring, n = 12; D: Pathological changes of the spinal cord were observed by H&E staining, n = 6; E: Cell apoptosis was evaluated by TUNEL staining, n = 6; F: ROS levels were determined by dihydroethidium staining, n = 6; G: Levels of TNF-α, IL-1β, and IL-6 in tissues were determined by ELISA, n = 6. *$P < 0.05$, **$P < 0.01$. Data A, E, and F were analyzed by one-way ANOVA, and data B, C and G were analyzed by two-way ANOVA, followed by Tukey's multiple comparison test.

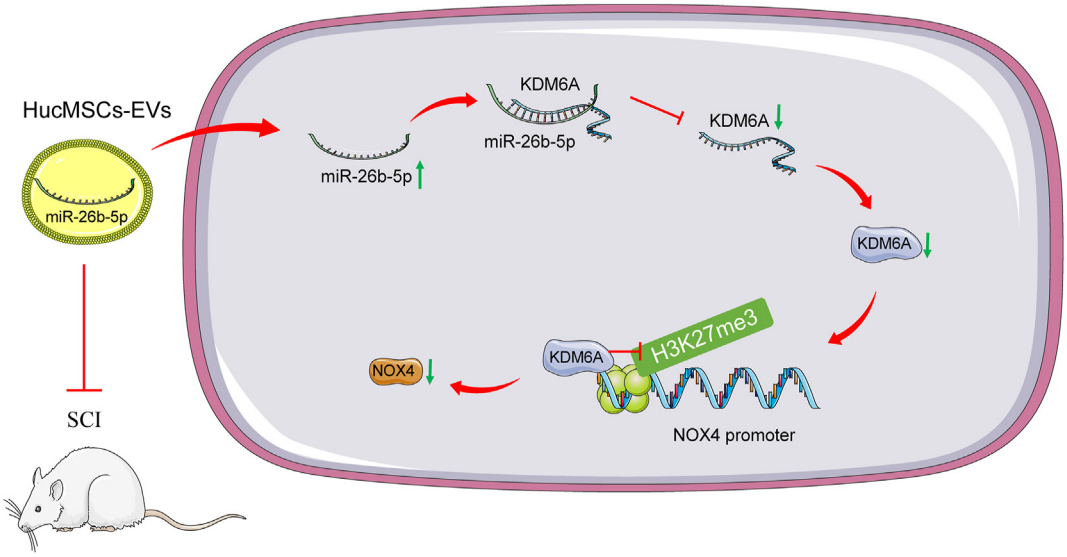

Fig. 9. Regulatory mechanism of HucMSCs-EVs in SCI. HucMSCs-EVs deliver miR-26b-5p into cells to upregulates miR-26b-5p to further repress KDM6A and elevate H3K27me3 at the NOX4 promoter, and ultimately inhibit NOX4 expression, thereby alleviating SCI.

downstream targets of miR-26b-5p and identify more therapeutic targets for SCI.

5. Conclusion

In summary, our findings for the first time demonstrated that MSCs-EVs transport miR-26b-5p into cells to repress KDM6A expression and reduce H3K27 demethylation-mediated promotion of NOX4, thereby repressing NOX4 and facilitating the functional recovery from SCI. Our study provided theoretical knowledge of the molecular mechanism of MSCs-EVs in the remission of SCI, which may facilitate the clinical application of MSCs-EVs into SCI treatment.

Declaration of competing interest

None.

References

[1] Anjum A, Yazid MD, Fauzi Daud M, Idris J, Ng AMH, Selvi Naicker A, et al. Spinal cord injury: pathophysiology, multimolecular interactions, and underlying recovery mechanisms. Int J Mol Sci 2020;21(20). https://doi.org/10.3390/ijms21207533.

[2] Russo GS, Mangan JJ, Galetta MS, Boody B, Bronson W, Segar A, et al. Update on spinal cord injury management. Clin Spine Surg 2020;33(7):258–64. https://doi.org/10.1097/BSD.0000000000000956.

[3] Quadri SA, Farooqui M, Ikram A, Zafar A, Khan MA, Suriya SS, et al. Recent update on basic mechanisms of spinal cord injury. Neurosurg Rev 2020;43(2):425–41. https://doi.org/10.1007/s10143-018-1008-3.

[4] Liu J, Gao J, Liang Z, Gao C, Niu Q, Wu F, et al. Mesenchymal stem cells and their microenvironment. Stem Cell Res Ther 2022;13(1):429. https://doi.org/10.1186/s13287-022-02985-y.

[5] Naji A, Eitoku M, Favier B, Deschaseaux F, Rouas-Freiss N, Suganuma N. Biological functions of mesenchymal stem cells and clinical implications. Cell Mol Life Sci 2019;76(17):3323–48. https://doi.org/10.1007/s00018-019-03125-1.

[6] Abels ER, Breakefield XO. Introduction to extracellular vesicles: biogenesis, RNA cargo selection, content, release, and uptake. Cell Mol Neurobiol 2016;36(3):301–12. https://doi.org/10.1007/s10571-016-0366-z.

[7] Liu WZ, Ma ZJ, Li JR, Kang XW. Mesenchymal stem cell-derived exosomes: therapeutic opportunities and challenges for spinal cord injury. Stem Cell Res Ther 2021;12(1):102. https://doi.org/10.1186/s13287-021-02153-8.

[8] Kim GU, Sung SE, Kang KK, Choi JH, Lee S, Sung M, et al. Therapeutic potential of mesenchymal stem cells (MSCs) and MSC-derived extracellular vesicles for the treatment of spinal cord injury. Int J Mol Sci 2021;22(24). https://doi.org/10.3390/ijms222413672.

[9] Munir J, Yoon JK, Ryu S. Therapeutic miRNA-enriched extracellular vesicles: current approaches and future prospects. Cells 2020;9(10). https://doi.org/10.3390/cells9102271.

[10] Correia de Sousa M, Gjorgjieva M, Dolicka D, Sobolewski C, Foti M. Deciphering miRNAs' action through miRNA editing. Int J Mol Sci 2019;20(24). https://doi.org/10.3390/ijms20246249.

[11] Liu W, Rong Y, Wang J, Zhou Z, Ge X, Ji C, et al. Exosome-shuttled miR-216a-5p from hypoxic preconditioned mesenchymal stem cells repair traumatic spinal cord injury by shifting microglial M1/M2 polarization. J Neuroinflammation 2020;17(1):47. https://doi.org/10.1186/s12974-020-1726-7.

[12] Khan NZ, Cao T, He J, Ritzel RM, Li Y, Henry RJ, et al. Spinal cord injury alters microRNA and CD81+ exosome levels in plasma extracellular nanoparticles with neuroinflammatory potential. Brain Behav Immun 2021;92:165–83. https://doi.org/10.1016/j.bbi.2020.12.007.

[13] Ge X, Tang P, Rong Y, Jiang D, Lu X, Ji C, et al. Exosomal miR-155 from M1-polarized macrophages promotes EndoMT and impairs mitochondrial function via activating NF-kappaB signaling pathway in vascular endothelial cells after traumatic spinal cord injury. Redox Biol 2021;41:101932. https://doi.org/10.1016/j.redox.2021.101932.

[14] Li C, Li Y, Lu Y, Niu Z, Zhao H, Peng Y, et al. miR-26 family and its target genes in tumorigenesis and development. Crit Rev Oncol Hematol 2021;157:103124. https://doi.org/10.1016/j.critrevonc.2020.103124.

[15] Icli B, Dorbala P, Feinberg MW. An emerging role for the miR-26 family in cardiovascular disease. Trends Cardiovasc Med 2014;24(6):241–8. https://doi.org/10.1016/j.tcm.2014.06.003.

[16] Acharya A, Berry DC, Zhang H, Jiang Y, Jones BT, Hammer RE, et al. miR-26 suppresses adipocyte progenitor differentiation and fat production by targeting Fbxl19. Genes Dev 2019;33(19–20):1367–80. https://doi.org/10.1101/gad.328955.119.

[17] Cheng L, Wang C, Yao F, Li Z, Liu W, Jing J. MicroRNA-26b inhibits oligodendrocyte precursor cell differentiation by targeting adrenomedullin in spinal cord injury. J Cell Physiol 2020;235(3):2429–40. https://doi.org/10.1002/jcp.29147.

[18] Penas C, Navarro X. Epigenetic modifications associated to neuroinflammation and neuropathic pain after neural trauma. Front Cell Neurosci 2018;12:158. https://doi.org/10.3389/fncel.2018.00158.

[19] Tran N, Broun A, Ge K. Lysine demethylase KDM6A in differentiation, development, and cancer. Mol Cell Biol 2020;40(20). https://doi.org/10.1128/MCB.00341-20.

[20] Ni S, Luo Z, Jiang L, Guo Z, Li P, Xu X, et al. UTX/KDM6A deletion promotes recovery of spinal cord injury by epigenetically regulating vascular regeneration. Mol Ther 2019;27(12):2134–46. https://doi.org/10.1016/j.ymthe.2019.08.009.

[21] Guo Z, Li C, Cao Y, Qin T, Jiang L, Xu Y, et al. UTX/KDM6A deletion promotes the recovery of spinal cord injury by epigenetically triggering intrinsic neural regeneration. Mol Ther Methods Clin Dev 2021;20:337–49. https://doi.org/10.1016/j.omtm.2020.12.004.

[22] Gao C, Yin F, Li R, Ruan Q, Meng C, Zhao K, et al. MicroRNA-145-Mediated KDM6A downregulation enhances neural repair after spinal cord injury via the NOTCH2/abcb1a Axis. Oxid Med Cell Longev 2021;2021:2580619. https://doi.org/10.1155/2021/2580619.

[23] Yu M, Wang Z, Wang D, Aierxi M, Ma Z, Wang Y. Oxidative stress following spinal cord injury: from molecular mechanisms to therapeutic targets. J Neurosci Res 2023. https://doi.org/10.1002/jnr.25221.

[24] Wang R, Liu Y, Jing L. MiRNA-99a alleviates inflammation and oxidative stress in lipopolysaccharide-stimulated PC-12 cells and rats post spinal cord injury. Bioengineered 2022;13(2):4248–59. https://doi.org/10.1080/21655979.2022.2031386.

[25] Khayrullina G, Bermudez S, Hopkins D, Yauger Y, Byrnes KR. Differential effects of NOX2 and NOX4 inhibition after rodent spinal cord injury. PLoS One 2023;18(3):e0281045. https://doi.org/10.1371/journal.pone.0281045.

[26] Guide for the Care and Use of Laboratory Animals. The national academies collection: reports funded by national institutes of health. 8th ed. Washington (DC); 2011.

[27] Nie H, Jiang Z. Bone mesenchymal stem cell-derived extracellular vesicles deliver microRNA-23b to alleviate spinal cord injury by targeting toll-like receptor TLR4 and inhibiting NF-kappaB pathway activation. Bioengineered 2021;12(1):8157–72. https://doi.org/10.1080/21655979.2021.1977562.

[28] Ding H, Gao S, Wang L, Wei Y, Zhang M. Overexpression of miR-582-5p inhibits the apoptosis of neuronal cells after cerebral ischemic stroke through regulating PAR-1/rho/rho Axis. J Stroke Cerebrovasc Dis 2019;28(1):149–55. https://doi.org/10.1016/j.jstrokecerebrovasdis.2018.09.023.

[29] Ragni E, Perucca Orfei C, Silini AR, Colombini A, Vigano M, Parolini O, et al. miRNA reference genes in extracellular vesicles released from amniotic membrane-derived mesenchymal stromal cells. Pharmaceutics 2020;12(4). https://doi.org/10.3390/pharmaceutics12040347.

[30] Livak KJ, Schmittgen TD. Analysis of relative gene expression data using real-time quantitative PCR and the 2(-Delta Delta C(T)) Method. Methods 2001;25(4):402–8. https://doi.org/10.1006/meth.2001.1262.

[31] Xiao X, Li W, Rong D, Xu Z, Zhang Z, Ye H, et al. Human umbilical cord mesenchymal stem cells-derived extracellular vesicles facilitate the repair of spinal cord injury via the miR-29b-3p/PTEN/Akt/mTOR axis. Cell Death Dis 2021;7(1):212. https://doi.org/10.1038/s41420-021-00572-3.

[32] Shao A, Tu S, Lu J, Zhang J. Crosstalk between stem cell and spinal cord injury: pathophysiology and treatment strategies. Stem Cell Res Ther 2019;10(1):238. https://doi.org/10.1186/s13287-019-1357-z.

[33] Nakazaki M, Morita T, Lankford KL, Askenase PW, Kocsis JD. Small extracellular vesicles released by infused mesenchymal stromal cells target M2 macrophages and promote TGF-beta upregulation, microvascular stabilization and functional recovery in a rodent model of severe spinal cord injury. J Extracell Vesicles 2021;10(11):e12137. https://doi.org/10.1002/jev2.12137.

[34] Liu W, Tang P, Wang J, Ye W, Ge X, Rong Y, et al. Extracellular vesicles derived from melatonin-preconditioned mesenchymal stem cells containing USP29 repair traumatic spinal cord injury by stabilizing NRF2. J Pineal Res 2021;71(4):e12769. https://doi.org/10.1111/jpi.12769.

[35] Wang Y, Xu H, Wang J, Yi H, Song Y. Extracellular vesicles in the pathogenesis, treatment, and diagnosis of spinal cord injury: a mini-review. Curr Stem Cell Res Ther 2022;17(4):317–27. https://doi.org/10.2174/1574888X17666220330005937.

[36] Deng ZZ, Chen YH. Research progress of MicroRNAs in spinal cord injury. J Integr Neurosci 2023;22(2):31. https://doi.org/10.31083/j.jin2202031.

[37] Li R, Zhao K, Ruan Q, Meng C, Yin F. Bone marrow mesenchymal stem cell-derived exosomal microRNA-124-3p attenuates neurological damage in spinal cord ischemia-reperfusion injury by downregulating Ern1 and promoting M2 macrophage polarization. Arthritis Res Ther 2020;22(1):75. https://doi.org/10.1186/s13075-020-2146-x.

[38] Zhao L, Jiang X, Shi J, Gao S, Zhu Y, Gu T, et al. Exosomes derived from bone marrow mesenchymal stem cells overexpressing microRNA-25 protect spinal cords against transient ischemia. J Thorac Cardiovasc Surg 2019;157(2):508–17. https://doi.org/10.1016/j.jtcvs.2018.07.095.

[39] Huang JH, Xu Y, Yin XM, Lin FY. Exosomes derived from miR-126-modified MSCs promote angiogenesis and neurogenesis and attenuate apoptosis after spinal cord injury in rats. Neuroscience 2020;424:133–45. https://doi.org/10.1016/j.neuroscience.2019.10.043.

[40] Zhou F, Zhang C, Guan Y, Chen Y, Lu Q, Jie L, et al. Screening the expression characteristics of several miRNAs in G93A-SOD1 transgenic mouse: altered

expression of miRNA-124 is associated with astrocyte differentiation by targeting Sox2 and Sox9. J Neurochem 2018;145(1):51–67. https://doi.org/10.1111/jnc.14229.
[41] Kang YC, Zhang L, Su Y, Li Y, Ren WL, Wei WS. MicroRNA-26b regulates the microglial inflammatory response in hypoxia/ischemia and affects the development of vascular cognitive impairment. Front Cell Neurosci 2018;12:154. https://doi.org/10.3389/fncel.2018.00154.
[42] Park J, Lee K, Kim K, Yi SJ. The role of histone modifications: from neurodevelopment to neurodiseases. Signal Transduct Targeted Ther 2022;7(1):217. https://doi.org/10.1038/s41392-022-01078-9.
[43] Dai H, Zhao N, Zheng Y. CircLDLR modulates the proliferation and apoptosis of vascular smooth muscle cells in coronary artery disease through miR-26-5p/KDM6A Axis. J Cardiovasc Pharmacol 2022;80(1):132–9. https://doi.org/10.1097/FJC.0000000000001275.
[44] Vermot A, Petit-Hartlein I, Smith SME, Fieschi F. NADPH oxidases (NOX): an overview from discovery, molecular mechanisms to physiology and pathology. Antioxidants 2021;10(6). https://doi.org/10.3390/antiox10060890.
[45] Bermudez S, Khayrullina G, Zhao Y, Byrnes KR. NADPH oxidase isoform expression is temporally regulated and may contribute to microglial/macrophage polarization after spinal cord injury. Mol Cell Neurosci 2016;77:53–64. https://doi.org/10.1016/j.mcn.2016.10.001.
[46] Siuda D, Zechner U, El Hajj N, Prawitt D, Langer D, Xia N, et al. Transcriptional regulation of Nox4 by histone deacetylases in human endothelial cells. Basic Res Cardiol 2012;107(5):283. https://doi.org/10.1007/s00395-012-0283-3.
[47] Liao Y, Gou L, Chen L, Zhong X, Zhang D, Zhu H, et al. NADPH oxidase 4 and endothelial nitric oxide synthase contribute to endothelial dysfunction mediated by histone methylations in metabolic memory. Free Radic Biol Med 2018;115:383–94. https://doi.org/10.1016/j.freeradbiomed.2017.12.017.